MATERIALS SCIENCE

Toughening stretchable fibers via serial fracturing of a metallic core

Christopher B. Cooper[1], Ishan D. Joshipura[1], Dishit P. Parekh[1]*, Justin Norkett[2], Russell Mailen[1†], Victoria M. Miller[2], Jan Genzer[1], Michael D. Dickey[1‡]

Tough, biological materials (e.g., collagen or titin) protect tissues from irreversible damage caused by external loads. Mimicking these protective properties is important in packaging and in emerging applications such as durable electronic skins and soft robotics. This paper reports the formation of tough, metamaterial-like core-shell fibers that maintain stress at the fracture strength of a metal throughout the strain of an elastomer. The shell experiences localized strain enhancements that cause the higher modulus core to fracture repeatedly, increasing the energy dissipated during extension. Normally, fractures are catastrophic. However, in this architecture, the fractures are localized to the core. In addition to dissipating energy, the metallic core provides electrical conductivity and enables repair of the fractured core for repeated use. The fibers are 2.5 times tougher than titin and hold more than 15,000 times their own weight for a period 100 times longer than a hollow elastomeric fiber.

INTRODUCTION

Tough materials found in nature maintain the structural integrity of many biological tissues against external loads. Collagen, e.g., toughens skin in a network comprising bundled fibers that quickly and effectively dissipate energy and prevent cuts from spreading (*1*). Human muscle is strengthened by the biomolecule titin, which unfolds reversibly to absorb tensile loads (*2*, *3*). These types of tissues not only need to be stretchable to accommodate tensile deformation but should also be tough to avoid mechanical failure. The ability to mimic these properties is important for both practical functions (e.g., packaging and protective equipment) and emerging applications that undergo elongation (e.g., stretchable electronics, soft robotics, and electronic skin).

Toughness of a material relates to the area under the stress-strain curve. Thus, materials that can elongate to large strains at large stress dissipate the most energy. Previous efforts to create tough materials have used sacrificial bonds that release hidden length when each bond breaks (*4*–*7*), structured architectures with different stable configurations that can trap energy (*8*–*10*), and interpenetrating polymer networks that have dissipative, reversible bonds (*11*–*13*). Here, we use an alternative strategy that combines a soft elastomer (which, in isolation, exhibits large elastic strains but maintains low levels of stress until right before failure) with a metal (which, in isolation, exhibits a large modulus but fails at catastrophically low strains). We use a core-shell fiber geometry comprising a core of gallium metal surrounded by an elastic shell of poly(styrene-ethylene butylene-styrene) (SEBS). The fibers achieve toughness by maintaining the high stress needed to deform the metallic core up to large strains enabled by the encasing elastomer. In this mechanism, energy dissipates via the repetitive, sequential breaking of the stiff metallic core, which is held together by an elastomeric shell that distributes the stress and maintains the mechanical integrity of the fiber. The approach here is a macroscopic analog to molecular dissipation (*14*) yet uses common elastomers without the need for sophisticated chemistry. Inspired by other tough composite lattices (*15*, *16*), the design provides a strategy to generate tough individual fibers in which the constituent with the higher modulus is encased within a polymer.

We consider these fibers "metamaterial-like" materials (although they could also be considered composites) because they derive their toughness in a manner similar to mechanical metamaterials, which use structured architectures to achieve atypical or markedly enhanced properties (*17*–*21*). For simplicity, we use "metamaterial" instead of metamaterial-like when describing the fibers from this point onward. The structural interplay between the fiber core and shell is reminiscent of "endoskeletons" (e.g., the combinations of bones and flesh in animals or the use of steel reinforcement in concrete). The human body, e.g., can dissipate energy from catastrophic loads via bone breakage but maintains overall structural continuity via the connectivity of the surrounding tissue. Whereas most energy-dissipating metamaterials operate in compression (*22*–*24*), the architecture reported here can absorb tensile loads up to 800% strain (compared to 30 to 150% strain for other tensile metamaterials) with an average toughness more than 2.5 times that of titin.

This approach also distinguishes itself from previous tensile-load–absorbing materials in several other notable ways. The fibers exhibit tunable "J-shaped" stress-strain behavior, a common biological mechanism to allow for natural extension in tissues while preventing damage from excessive strains (*25*), with the added benefit of dissipating more energy at high strains instead of mechanically failing. In addition, the ability to melt and solidify the metallic core allows the fiber to regain strength after straining through a repairing process and to quickly and reversibly alternate between soft and rigid mechanical properties, which is similar to the collagenous connective tissues of sea cucumbers (*26*, *27*). These types of mechanisms are desirable for tuning the mechanical properties of stretchable electronics, soft robots, and other emerging deformable devices (*28*–*30*).

Moreover, the fibers use a simple architecture with a high aspect ratio geometry (length to width) at all levels of strain, unlike other metamaterials that feature complex designs or larger cross sections at low strains, to incorporate hidden length. This design enables a wider range of applications including incorporation into textiles, fiber-reinforced composites, and braided fibers. Working with liquid gallium also has the advantage that the gallium core could be injected and even

[1]Department of Chemical and Biomolecular Engineering, North Carolina State University, Raleigh, NC 27695-7905, USA. [2]Department of Materials Science Engineering, North Carolina State University, Raleigh, NC 27695-7905, USA.
*Present address: IBM Research, 257 Fuller Road, Albany, NY 12203, USA.
†Present address: Department of Aerospace Engineering, Auburn University, Auburn, AL 36849-5338, USA.
‡Corresponding author. Email: mddickey@ncsu.edu

moved within a vasculature before solidification, thus enhancing the simplicity and scalability of the fabrication process (*31*). The gallium core also endows the fibers with beneficial metallic electrical and thermal conductivity, as well as high optical reflectivity, thus making them potentially useful for sensors, interconnects, antennas, and other radio frequency and optical structures. This paper characterizes these tough fibers and the unique interplay between the sequential energy dissipation afforded by the sacrificial fracture of the metallic core and the cohesion and strain localization provided by the elastomeric shell.

RESULTS

Characterization of the tough metamaterial fibers

Figure 1A depicts a schematic of a core-shell fiber and a cross-sectional view of the fiber (for a more detailed schematic, see fig. S1). The fiber consists of an elastic SEBS polymer shell (which, in isolation, has a low modulus, high strength, and high strain at break) that surrounds a stiff gallium metallic core (which, in isolation, features a high modulus, high strength, and low strain at break). Unless otherwise stated, the outer diameter (OD) of the fiber is 1.2 mm and the inner diameter (ID) is 0.85 mm. Gallium melts with mild heating (T > 30°C), allowing it to be injected into the core of the fiber using a syringe with mild pressure (~1 kPa) that does not distort the fiber shell (*32*).

The schematic in Fig. 1A illustrates the basic principles of the energy-dissipating fiber. At low strains, the fiber features a high modulus (defined primarily by the metallic core) and deforms uniformly, until a break occurs in the core. Normally, a break to a metallic fiber or wire would be catastrophic. However, here, the presence of the polymer shell creates a "polymer bridge" (i.e., a region of polymer with no metallic core) that connects and transfers force between the two separated segments of core metal. As the macroscopic strain of the fiber increases, more breaks occur in the metallic core, and each break introduces an additional polymer bridge supplied by the shell. The failure of the entire fiber eventually arises from the failure of the polymeric shell at high strain.

Figure 1B compares the force versus strain responses of a solid gallium rod, an empty SEBS fiber, and a Ga-SEBS metamaterial fiber (see fig. S2 for stress-strain data). In Fig. 1B, each sudden decrease in force corresponds to a break in the metallic core of the Ga-SEBS fiber, after which a polymer bridge forms from the encasing polymer. After each break, the force needed to maintain a constant rate of extension increases steadily as the bridge is strained, until eventually the metallic core fractures again and the cycle repeats itself. During these cycles, the strain localizes primarily in the polymer bridges between the breaks, which keeps the overall stress high regardless of the macroscopic strain. This behavior generates a sawtooth-shaped curve centered about the force needed to break the metallic core (see note S1 for additional details) and provides an effective and continuous energy dissipation method. The fiber sustains approximately the same force as the force needed to break the metallic core, but for almost six times the amount of strain.

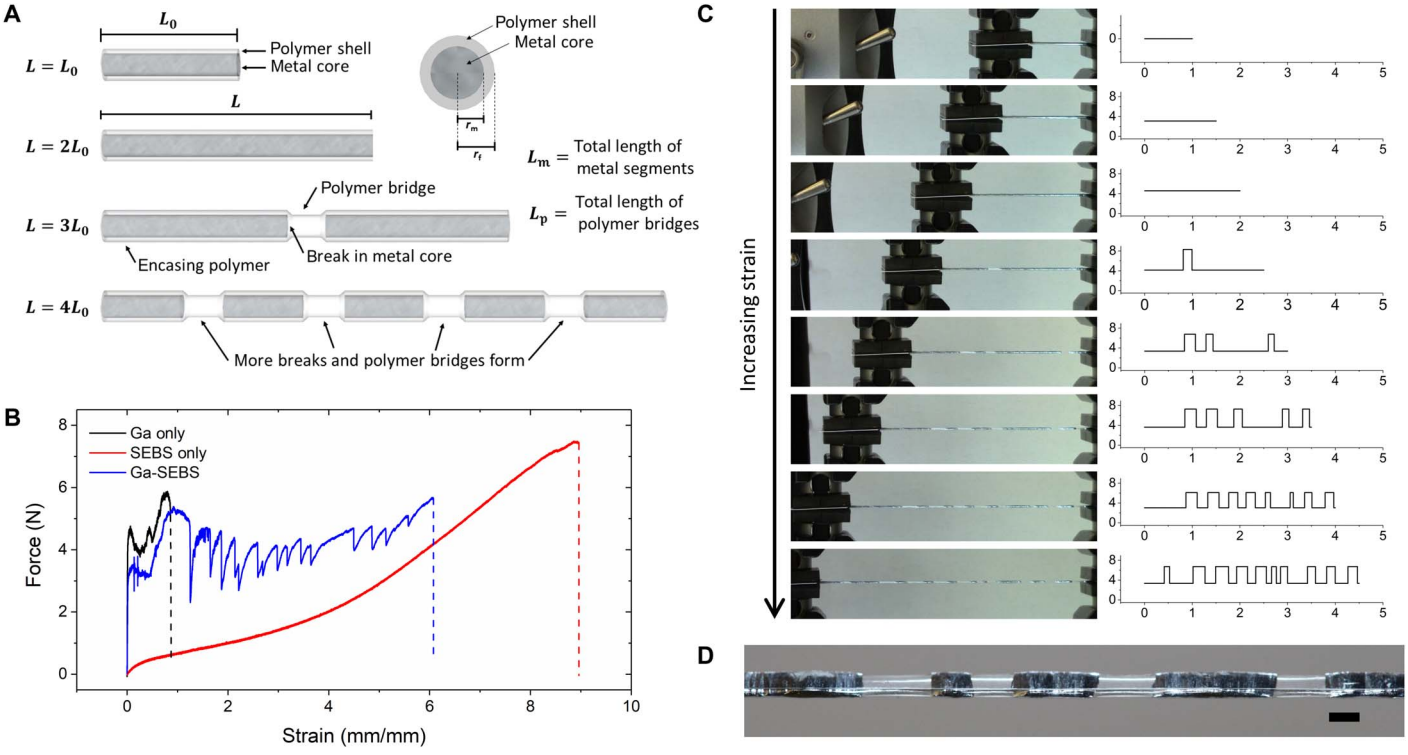

Fig. 1. A hollow polymer fiber filled with solid gallium creates a tough metamaterial core-shell fiber. (**A**) Schematic of the metamaterial (Ga-SEBS) fiber being strained. By inducing multiple breaks in the gallium core, the fiber dissipates large amounts of tensile energy at a near-constant rate. (**B**) Force versus strain for a solid gallium core (black), a hollow SEBS fiber (red), and a Ga-SEBS fiber (blue). (**C**) Images of a Ga-SEBS fiber from 0 to 350% strain in intervals of 50% strain accompanied by corresponding stress position graphs. The ordinate depicts engineering stress (in MPa; normalized by the initial fiber cross-sectional area), and the abscissa denotes position (in mm/mm; normalized by the initial fiber length) where zero is the leftmost part of the fiber. For scale, the initial fiber length is 27 mm. (**D**) A close-up image of a fiber at 800% strain. Scale bar, 1 mm. Photo credit: Christopher B. Cooper, North Carolina State University.

For the high-modulus metallic core to serve as the sacrificial material (which gives the fibers their high toughness), the force needed to break the metallic core must be less than the force required to break the polymer shell. Conversely, since the energy dissipation in the fiber arises from the repeated sacrificial fracture of the metallic core, the force required to break the metallic core directly determines the overall toughness of the fiber. Optimization of these factors can be accomplished by tuning the geometry (i.e., cross-sectional area) and material properties (i.e., tensile strength) of each component in the fiber. Here, we use single crystals of gallium, which are soft because they do not exhibit solid solution strengthening or grain boundary strengthening. In addition, they have thermally activated deformation mechanisms because gallium's melting point is just above room temperature (*33*). The fiber dimensions (1.2-mm OD and 0.85-mm ID) give a Ga-to-SEBS cross-sectional area ratio of 1 compared to the Ga-to-SEBS tensile strength ratio of 0.92 (based on the values reported in Table 1). These dimensions allow the metallic core to fracture multiple times while maximizing the amount of energy dissipated by the metallic core with each break and thus maximizing the overall toughness of the fibers.

Table 1 lists the values for the initial modulus, tensile strength, strain at failure, and toughness at 450% strain for a solid gallium core, a hollow SEBS fiber, and a Ga-SEBS fiber (additional data provided in table S1). At low strains, the gallium core dominates the mechanical response of the fibers, as shown in Fig. 1B, and can be further seen by comparing the moduli of the different materials listed in Table 1. The average modulus of the core-shell fibers is much closer in magnitude to the modulus of a solid gallium rod. The difference in the tensile strength of the solid gallium rod and the Ga-SEBS fiber, despite reaching roughly the same maximum force (as shown in Fig. 1B) is due to the difference in their cross-sectional areas. The force on the solid gallium rod is normalized only by the cross-sectional area of the gallium, while the force on the Ga-SEBS fiber is normalized over the cross-sectional area of both the gallium core and the SEBS shell, although the latter does not contribute to the force at low strains.

The average toughness of the metamaterial fibers, reported in Table 1, was calculated by integrating each stress-strain curve and was further validated by linear regression on the aggregated stress-strain data (see fig. S3 for more details). The fibers maintain a near-constant stress of 3.9 MPa for an average strain of 450% and achieve a maximum toughness of 25 MJ/m^3. Comparing the toughness of the fibers to a hollow SEBS fiber stretched to 450% reveals that the metamaterial fiber exhibits nearly twice the toughness (i.e., it absorbs almost twice as much energy as a hollow SEBS fiber strained by the same amount). These results highlight an important underlying distinction between the energy dissipation mechanisms of the hollow SEBS fiber and the metamaterial fiber; the former only dissipates energy at very high strains, while the latter dissipates energy at a near-constant rate. We used the density of the metamaterial fibers (3410 kg/m^3) and the toughness values reported above to calculate the average specific energy absorption (5.1 kJ/kg) and the maximum specific energy absorption (7.5 kJ/kg) for the tough fibers.

Figure 1C displays a series of images of a metamaterial fiber as it is strained, beginning at 0% strain and increasing in 50% strain increments up to 350% strain. Movie S1 displays the behavior of the fiber as it is strained in real time. While straining the fiber fractures the gallium core, the encasing polymer maintains the overall structural integrity of the fiber. The respective stress position distribution is given on the right of each image. The ordinate in Fig. 1C denotes engineering stress (in MPa; i.e., the force normalized by the fiber's initial cross-sectional area), and the abscissa denotes position (in mm/mm; normalized by the fiber's initial length) where zero is the leftmost end of the fiber. Once the metallic core has fractured (see Fig. 1D), the fiber consists of regions with and without metallic cores (we call the latter polymer bridges). Since the cross-sectional area of a polymer bridge is always smaller than that of the core-shell fiber (which includes the areas of both the polymer shell and the metallic core), the stress is always higher in the polymer bridges, which implies that stress is not distributed uniformly along the length of the fiber. For this reason, it is conceptually easier to imagine the system in terms of force, which is constant along the length of the fiber.

To learn more about the underlying mechanisms behind the metamaterial behavior, we analyzed video footage of the fiber extending (e.g., movie S1). Figure 2A tracks the repeated fracture of the metallic core into smaller segments as the overall strain of the fiber increases. The plot contains bars that represent the length of the metal segments within the fiber (normalized by the initial length of the metal). Initially, the fiber contains only one long metal segment that extends to a flat, knife-edge structure until 125% strain, at which point the first fracture occurs. Each time a new (smaller) segment forms via a fracture, a newly colored bar appears in the chart. In addition, the stress-strain curve for the same fiber is overlaid onto the graph using the secondary ordinate. The plot helps visualize that each sharp drop in stress corresponds to a break in the metallic core. In addition, as the strain increases, the size of each gallium segment becomes more uniform in length. The small piece of gallium that appears at a strain of 2.5 mm/mm at the top of the bar graph is due to a break close to the grip of the extensometer.

Figure 2B plots the normalized length of the metal (red), the fiber (black), and the polymer bridges (blue) versus macroscopic strain. The total normalized length of the metal increases linearly with that of the fiber until the first break in the metal occurs at a strain of 1.25 mm/mm. After the break, the sum of the metal segment lengths stays nearly constant. Thus, instead of the constituent materials of the fiber straining uniformly after the first break, subsequent increases in macroscopic strain are maintained solely by the elongation of the polymer bridges that appear between the metal segments after each break. The length

Table 1. Comparison of mechanical properties of metamaterial fiber to constituent materials.

	Initial modulus (MPa)	Tensile strength (MPa)	Strain at failure (%)	Toughness at 450% strain (MJ/m^3)
Ga only	1800	12.4	60	5.3*
SEBS only	3	13.5	860	10.2
Ga-SEBS	800	5.9	450	17.3

*Breaks at 60% strain.

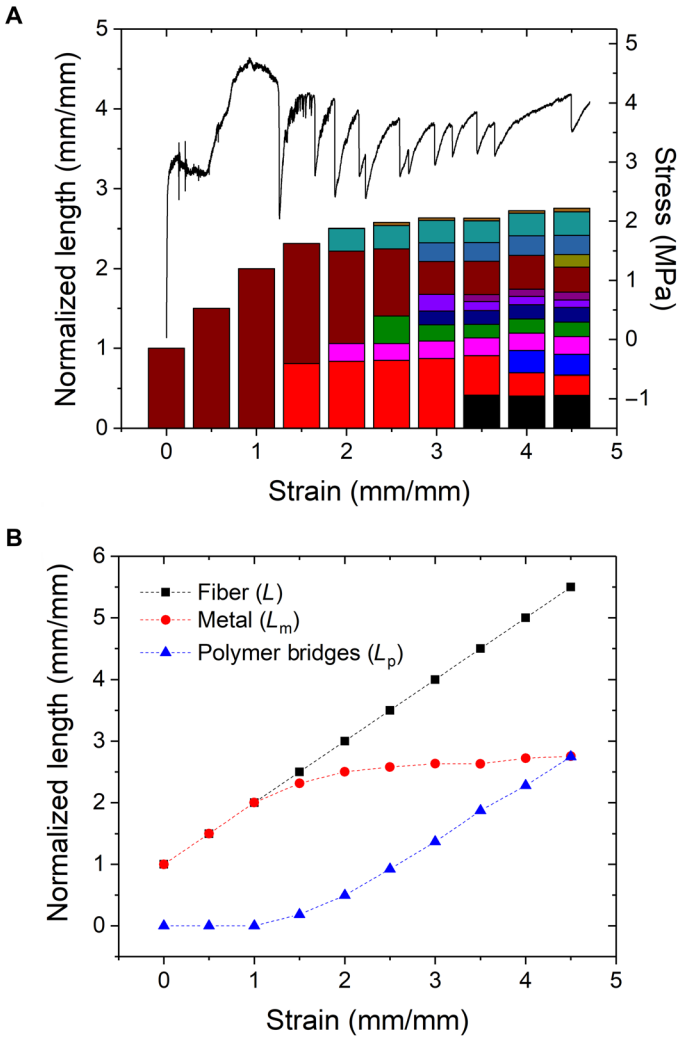

Fig. 2. Characterization of metamaterial fiber behavior. (**A**) Stacked graph of normalized length of gallium segments (left ordinate) at 50% strain intervals for a fiber up to 450% strain. Different colors represent different segments of metallic core within a single fiber. A stress-strain curve for the fiber is overlaid (right ordinate). (**B**) Graph of the normalized total length of metal segments (red circles) and polymer bridges (blue triangles) compared to the normalized total fiber length (black squares). The dashed lines guide the eye.

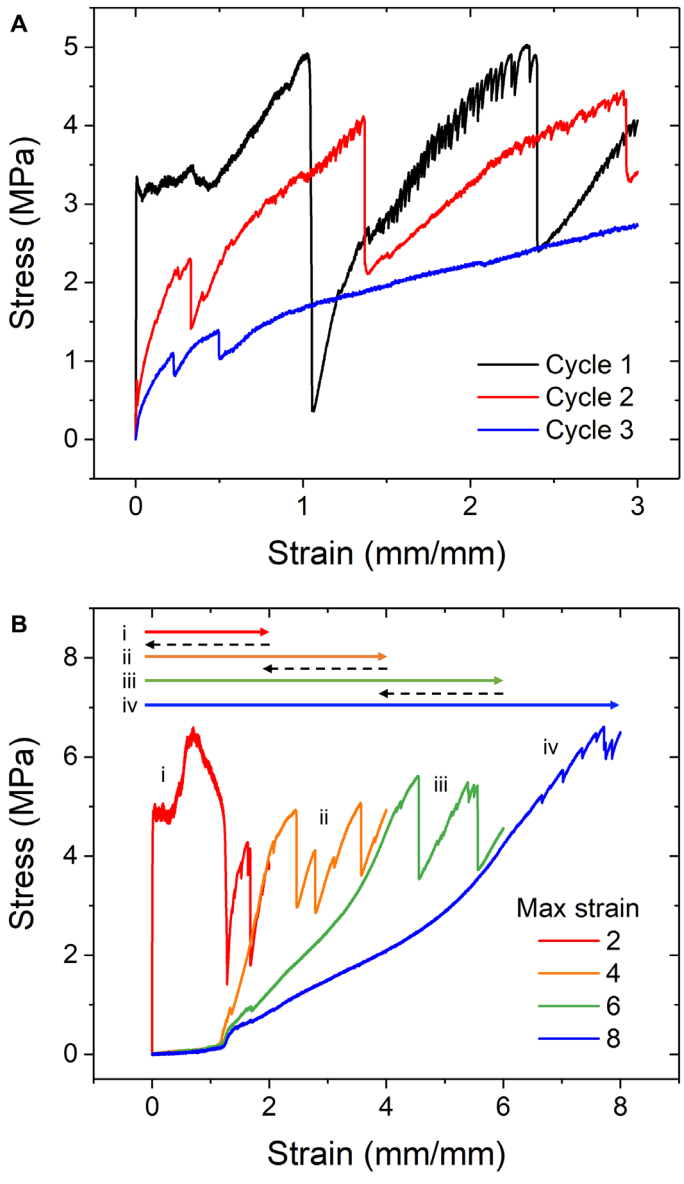

Fig. 3. Repairing and J-shaped stress behavior of metamaterial fibers. (**A**) Repairing of the Ga-SEBS fibers is demonstrated by straining a fiber to 300% strain for three cycles with heating in between each cycle to melt and then solidify the gallium core. (**B**) A single fiber is strained from 0 to 200% strain (reported in the legend as a maximum strain of 2), relaxed, strained to 400%, relaxed, strained to 600%, relaxed, and then lastly strained to 800% to exhibit tunable J-shaped stress behavior.

of these polymer bridges is zero until the first break in the metallic core occurs, thus causing the first polymer bridge to appear.

Repairing and J-shaped stress-strain behavior

The fibers can be repaired (and thus be strained repeatedly) by allowing the metallic core to melt and resolidify between cycles. Figure 3A reports the performance of a single fiber that has been tested in such a way. The fiber has been strained to 300% and then relaxed to 0% strain. Heating the fiber above 30°C melts the gallium, which resolidifies at room temperature. The fiber is then strained again to 300% strain. While the results show that the fiber can be used repeatedly, the overall strength and toughness of the fiber decay with each cycle. The ends of the fiber are damaged by the extensometer grip, allowing liquid gallium to escape during the repairing process and introducing pockets of air into the reformed metallic core, which artificially weaken the overall strength and toughness of the fiber. Hollow SEBS fibers are known to exhibit minimal hysteresis over many cycles (*34*). Thus, if the fiber ends could be sealed to withstand the extensometer grips, then the demonstrated reversibility of the fiber would likely increase.

The fibers can also be tuned to exhibit the J-shaped stress behavior observed in many biological tissues (i.e., tuned to allow a certain amount of strain at low stress before rapidly increasing to high stress to prevent damage from further strain) (*25*). Figure 3B demonstrates the ability of the fibers to be tuned to exhibit this behavior at different levels of strain, with the added benefit of dissipating more energy at the high stress instead of simply failing. To demonstrate this behavior, a single fiber is strained to 200% strain, relaxed back to 0%, strained to 400%, relaxed

back to 0%, strained to 600%, relaxed back to 0%, and then strained to 800%. In each case, after relaxation, the fiber resumes metamaterial behavior after reaching the maximum strain of the previous cycle. Thus, by prestraining, fibers can be tuned by intentionally introducing fractures to allow some desirable level of strain at low stress, after which the fiber exhibits metamaterial behavior and dissipates energy at high stress.

Modeling the behavior of a metamaterial fiber during elongation

To better understand the interplay between the metallic core and the polymer shell, we developed a mathematical model to estimate the theoretical distribution of stresses and strains in different regions of the fiber as a function of macroscopic strain. Once the metal breaks, there are regions with and without a metallic core in the fiber and these regions no longer strain uniformly. The amount of strain experienced by the polymer bridges (i.e., regions with no metallic core) is further complicated by the fact that the polymer in the polymer bridges comes from the "slipping" of the encasing polymer (i.e., the polymer surrounding a metallic core). We sought to understand this behavior by considering two phenomena that must be true: (i) At any cross section of the fiber, the net force must be equal to the force exerted by the grips of the extensometer at the ends of the fiber. (ii) The sum of the lengths of the metal segments and the polymer bridges must always equal the total length (L) of the fiber.

A full derivation of the equations used in the model is given in note S2. Here, we outline the general process. At a given macroscopic strain (where the initial fiber length, the extended fiber length, the length of the polymer bridges, the length of the metal segments, and the force measured by the extensometer are all measured), we can readily calculate the engineering stress in the fiber and the polymer bridges. On the basis of the mechanical properties of the polymer, we can determine the localized strain in the polymer bridges from the measured force (see fig. S7).

At this point, we would like to compare the amount of polymer in the polymer bridges and the encasing shell; however, we cannot do so directly, since these regions are at different strains. Thus, we instead evaluate the amount of polymer in each region at hypothetical zero strain (i.e., its length if it elastically recovered to its original state in the absence of stress). We call this the initial length of the polymer, where the sum of the initial length of polymer bridges (i.e., regions without metal) and encasing polymer (i.e., regions with metal) is constant and equal to the initial length of the polymer (i.e., the initial fiber length). Physically, the initial length of a polymer bridge represents the magnitude by which the encasing polymer has transferred (or "slipped") between the metallic core segments. Movie S2 provides a real-time example of the encasing polymer slipping past a metallic core fracture to lengthen a polymer bridge. Since the encasing polymer continues to slip after a break in the metallic core, the initial length of the polymer bridges is not static, but rather, it is a function of macroscopic strain.

Once the initial length of the encasing polymer is known, it is possible to estimate the localized strain and stress in the encasing polymer. The remainder of the force in these segments must be sustained by the metal; thus, we can then use this information to estimate the engineering stress in the metal. The resulting model can be used to estimate stresses and strains throughout the fiber as a function of macroscopic strain. To do so, we inputted the stress-strain data from a metamaterial fiber and made the additional assumption that, after the first break in the metallic core, the total length of metallic core is constant (justified by the experimental findings reported in Fig. 2B). We then calculated the respective stresses and strains in different regions of the fiber.

Figure 4A displays the engineering stress in the fiber (measured by the extensometer) and the estimated engineering stresses in the metal, the encasing polymer, and the bridging polymer as functions of global strain. In regions with metal segments, the metallic core bears most of the stress, while the encasing polymer bears only a small amount of stress. However, this relationship changes as the global strain increases because the strain of the encasing polymer increases as more of the encasing polymer transfers to the polymer bridges. The plot reveals that the engineering stress in the encasing polymer increases monotonically and almost linearly despite the marked nonlinear stress profiles of the other regions of the fiber. This indicates that the encasing polymer continuously transfers into the polymer bridges (which steadily increases the stress in the remaining encasing polymer) as opposed to slipping in large chunks only when a break occurs. This suggests that the elastomeric

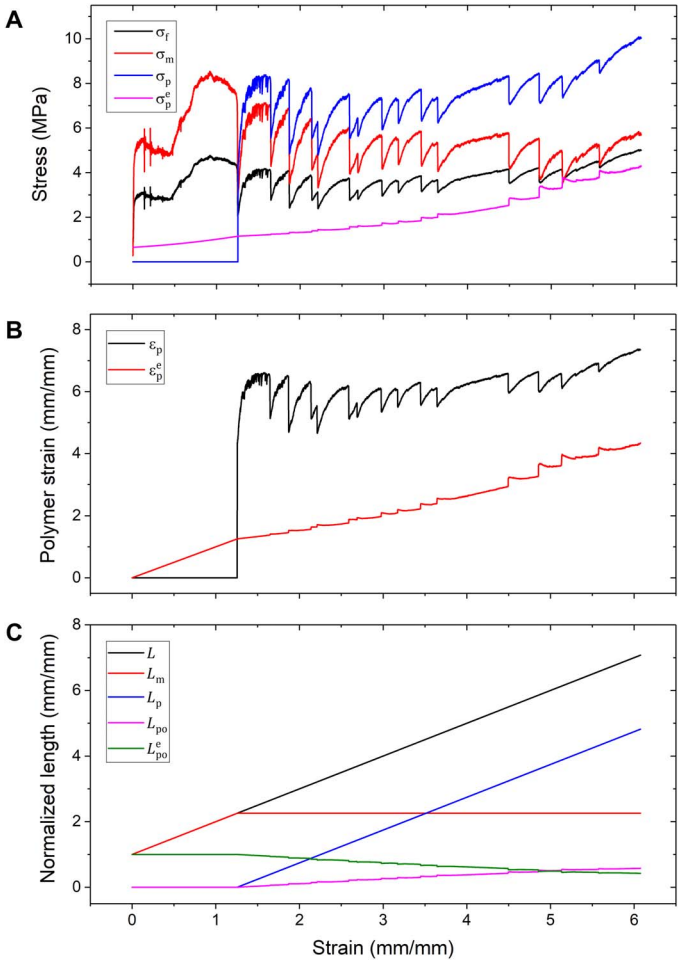

Fig. 4. A physical model of a metamaterial fiber. (**A**) Measured (i.e., known) engineering stress in the fiber (σ_f) and estimated (i.e., theoretical) engineering stresses in the metal (σ_m), polymer bridges (σ_p), and encasing polymer (σ_p^e) as functions of macroscopic strain. (**B**) Estimated average strain in the polymer bridges (ε_p) and the encasing polymer (ε_p^e) as functions of macroscopic strain. (**C**) Total measured length (L) of the fiber, along with estimated lengths of the metal (L_m) and polymer bridges (L_p), and estimated initial lengths of the polymer bridges (L_{po}) and encasing polymer (L_p^e) all as functions of macroscopic strain. Estimated values are determined directly from the model (see all equations and full derivation in note S2).

outer shell continually redistributes stress along the length of the fiber to prevent mechanical failure.

Figure 4B shows how the localization of stress plotted in Fig. 4A affects the estimated strains in the polymer bridges and the encasing polymer. The average strain in the polymer bridges remains almost constant, while the strain in the encasing polymer rises steadily as macroscopic strain increases. Thus, after a break in the fiber core, a small amount of encasing polymer creates a polymer bridge and immediately elongates to high local strain as it bears the full force exerted by the extensometer. As more of the encasing polymer slips into the polymer bridge, the slipping polymer elongates to the high local strain. Thus, the increasing length of the polymer bridges over time is the result of the slipping of additional encasing polymer into the bridges (as opposed to the polymer bridges themselves straining further, which would cause failure at prematurely low global strains). Figure 4C provides further evidence of this mechanism by plotting the estimated normalized lengths of the fiber, metal segments, polymer bridges, initial bridging polymer, and initial encasing polymer as macroscopic strain increases. The initial length of the polymer bridges increases linearly with macroscopic strain, in accordance with a decrease in the initial length of the encasing polymer.

The model predicts that the behavior of the fiber should be independent of the overall fiber diameter (holding the ratio between the ID and OD constant). We tested this hypothesis with fibers with a narrow range of diameters (ODs of 0.8, 0.9, and 1.2 mm) and found that the performance of the fibers was similar (see fig. S4). We also strained two fibers simultaneously, and both fibers exhibited metamaterial behavior above 500% strain (see fig. S5). These results suggest that the fibers could be scaled in overall size or combined in more complex structures to meet performance requirements; however, further research on the scalability of the fibers is necessary. Last, we fabricated metamaterial fibers using a gallium core and a silicone polymer shell and observed metamaterial behavior that enhanced toughness compared to a hollow silicone fiber up to 500% strain (see fig. S6), indicating that the unique mechanical behavior described is not limited to the Ga-SEBS material system.

Several noteworthy observations cannot yet be explained fully from the model. First, the metamaterial fibers fail at a lower strain and force than polymer fibers with a hollow core (see Fig. 1B). This observation combined with the variation of the strain at failure (typically 300 to 650%) for the metamaterial fibers suggests that the fibers may be failing at rough spots on the fractured metal segments. Alternatively, it is possible that we are underpredicting the local strain and thus true stress in the polymer bridges or that there are some effects related to a nonuniaxial stress state that cause premature failure of the fiber. Second, the length of the broken metal segments seems to tend toward a characteristic length (~6 mm), which is consistent with previous research that reported controlled fragmentation by cold drawing composite fibers (*35*). This result could be due to a certain minimum length of metal being necessary to effectively transfer stress between the polymer shell and the metallic core. Note that the model considers only axial forces and treats the fractured fiber as two distinct but otherwise homogeneous components: (i) segments of metallic cores encased by an elastomeric shell and (ii) hollow polymer bridges. However, there is a nontrivial third region where the stress transfers between the two components, which should be addressed with future revisions of the model.

Postmortem analysis of strained fibers

We also aimed to identify the mechanism by which gallium elongates and fractures inside the fiber. We noticed striations on the surface of the metal during elongation, which are thought to be slip bands, or material regions where many dislocations traversed the metallic crystal in a single crystallographic plane. These slip bands were investigated in greater detail via a postmortem analysis of strained fiber specimens to reveal information about the active deformation mechanisms in the gallium fibers.

All examined fibers exhibited consistent slip traces along their whole length, indicating that they are single crystals. No stray grains were observed; solidification appears to have originated from a single nucleus (i.e., the inserted copper wire) in each fiber. With solidification occurring very close to the melting point of gallium, the driving force for nucleation is very low, thus forming few competing nuclei. In addition, all examined fibers flattened during deformation and necked down to a "knife edge," suggesting that a single slip system dominated the deformation behavior of the crystal.

Solidified gallium metal has an orthorhombic crystal structure (D_{2h}^{18}) with an eight-atom unit cell having dimensions unit of $a = 4.5259$ Å, $b = 4.5199$ Å, and $c = 7.6603$ Å (*36*). A growth direction near the b axis, [010], was determined for the fiber using electron backscatter diffraction (EBSD). This is not surprising, as the b direction is also the elastically softest direction (*37*), which is commonly a favorable growth direction during the solidification of metals (*38*).

We compared the geometry of all possible slip traces of gallium to the experimentally observed slip traces. On the basis of this analysis, the most likely slip system is $[011](0\bar{1}1)$. This slip system both closely matches the observed slip traces and has the highest Schmid factor (0.438) of any reported deformation mode in gallium, thus making it the most geometrically favorable. Others have observed this slip system in similarly oriented fibers (*36*, *39*). Assuming that this slip system was active in all fibers, critical resolved shear stresses for deformation between 3.16 and 6.04 MPa were obtained, which agree well with the mean value of 5 MPa reported previously (*36*).

In addition, we compared the deformation of gallium with and without a polymer shell. An individual gallium rod (i.e., the core without a polymer shell) fractures on average at a strain of 60%. This result suggests that the gallium rod itself can elongate plastically to 60% strain before failing; however, the first break in a metamaterial fiber (i.e., the same gallium core surrounded by a SEBS polymer shell) occurs on average at a strain of 145%, more than twice that of an unsheathed gallium core. This observation suggests that the SEBS is stabilizing the deformation of the gallium core, delaying the onset of shear localization and therefore delaying fracture. The delay of shear localization in elastomer-coated metal specimens has been reported and explained in detail (*40*).

Demonstration of an energy-dissipating fiber

Last, to help visualize the capabilities of the metamaterial fiber, we compared the performance of the fiber to a hollow SEBS fiber under a load of 5.5 N, which is more than 15,000 times the weight of the metamaterial fiber (see movie S3). Figure 5 (A to C) shows both fibers when the load is initially applied, 1 s after and 15 s after, respectively. The metamaterial fiber strains slowly and constantly for more than 15 s, before failing at around 500% strain. Compared to the hollow SEBS fiber, which hits the substrate almost immediately, the metamaterial fiber holds the load for a period more than 100 times longer. This slow, steady strain rate highlights the high sequential energy absorption of the metamaterial fiber at all levels of strain compared to the low-energy absorption (and thus quick extension) of the hollow SEBS fiber.

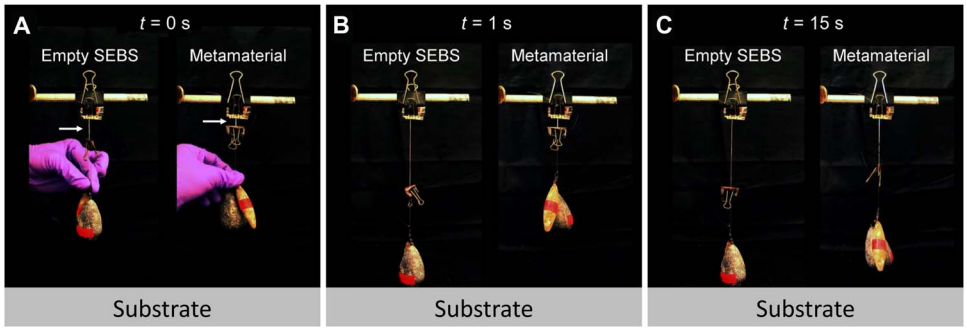

Fig. 5. A demonstration of the metamaterial fiber. (**A**) A load of 5.5 N is applied to both a hollow SEBS fiber (left) and a metamaterial fiber (right). (**B**) One second later, the SEBS fiber has fully extended and hit the substrate, while the metamaterial fiber still holds the load and continues to slowly extend. (**C**) Fifteen seconds later, the metamaterial fiber has elongated substantially and continues to hold the load. Photo credit: Christopher B. Cooper, North Carolina State University.

DISCUSSION

This paper discusses the creation of tough (energy-dissipating) metamaterial fibers that maintain high levels of stress for large tensile strains by using the sacrificial fracture of a high-modulus, stiff core and the cohesion of a low-modulus, elastic shell. These fibers can dissipate energy over large strains, which may be desirable for packaging or safety gear. The use of a low–melting temperature metallic core has several benefits including ease of fabrication (e.g., injection), the ability to heal the fractured structures for multiple uses, the ability to change the modulus markedly via phase change, and the ability to integrate electronic functionality (e.g., electrodes, sensors, and antennas). It is also straightforward to create "J-shaped" stress-strain behavior in the fibers, which may be useful for mimicking tissue mechanics in soft robotics and stretchable electronics. While this work focuses on the properties of a gallium core and a SEBS shell, toughening materials by the sacrificial fracture of encased high-modulus materials could be applied to a broad range of materials and geometries, including 2D or even 3D structures. For example, it may be desirable to use stiffer core materials with thinner cross sections to improve flexibility while maintaining the overall energy-dissipating force necessary to fracture the core. Overall, these metamaterial fibers represent an example of a promising new class of materials that achieve toughness in tension through sacrificial fracture of high-modulus constituents.

MATERIALS AND METHODS

Metamaterial fiber fabrication

Hollow poly(SEBS) fibers (Kraton G1643) were created by melt spinning, and subsequently, their hollow cores were filled fully with molten gallium via injection with a plastic needle-tipped syringe at ambient pressure. In this way, the gallium core matched the inner dimensions of the polymer fiber (0.85 mm) as closely as possible. Previous studies have discussed the adhesion of molten metal with polymeric substrates (*41*). The gallium was then solidified at room temperature by insertion of a copper wire (previously sanded with sandpaper and dipped in 0.1 M hydrocholoric acid) into the molten gallium at one end of the fiber while the fiber was held straight by taping each end lightly to cardstock. The ends of the fiber were sealed with NOA 63 optical adhesive.

Mechanical testing

All tensile strain experiments were carried out using an Instron extensometer at a strain rate of 1% per second. Fibers were held at each end by the pressurized grips of the extensometer at a lower operating pressure to prevent fiber ends from being crushed. All experiments were conducted at room temperature.

Postmortem analysis of strained fibers

Slip traces and fracture regions of the gallium core were examined via optical microscopy. The fiber orientation was measured using EBSD on the deformed specimen after manual removal of the polymer shell. The EBSD data were processed using the MTEX Toolbox for MATLAB to determine the active slip system (*42*).

SUPPLEMENTARY MATERIALS

Supplementary material for this article is available at http://advances.sciencemag.org/cgi/content/full/5/2/eaat4600/DC1

Note S1. Quantitative characterization of the metamaterial fiber stress-strain behavior.
Note S2. Full derivation of model.
Fig. S1. Detailed schematic of metamaterial fiber behavior.
Fig. S2. Stress-strain curves for Ga-only, SEBS-only, and Ga-SEBS fibers.
Fig. S3. Linear regression of aggregated stress-strain data from metamaterial fibers.
Fig. S4. Scalability of metamaterial fibers.
Fig. S5. Simultaneous straining of two metamaterial fibers.
Fig. S6. Metamaterial fiber composed of a gallium core and a silicone polymer shell.
Fig. S7. Second-order polynomial regression for a hollow SEBS fiber.
Fig. S8. Optical images of a relaxed metamaterial after straining.
Table S1. Comparison of mechanical properties with SDs, 95% confidence intervals, and sample sizes.
Movie S1. Elongation of a metamaterial fiber.
Movie S2. Slipping mechanism for the formation of polymer bridges.
Movie S3. Demonstration of a metamaterial fiber.

REFERENCES AND NOTES

1. W. Yang, V. R. Sherman, B. Gludovatz, E. Schaible, P. Stewart, R. O. Ritchie, M. A. Meyers, On the tear resistance of skin. *Nat. Commun.* **6**, 6649 (2015).
2. L. Tskhovrebova, J. Trinick, Titin: Properties and family relationships. *Nat. Rev. Mol. Cell Biol.* **4**, 679–689 (2003).
3. M. Rief, M. Gautel, F. Oesterhelt, J. M. Fernandez, H. E. Gaub, Reversible unfolding of individual titin immunoglobulin domains by AFM. *Science* **276**, 1109–1112 (1997).
4. R. Passieux, L. Guthrie, S. H. Rad, M. Lévesque, D. Therriault, F. P. Gosselin, Instability-assisted direct writing of microstructured fibers featuring sacrificial bonds. *Adv. Mater.* **27**, 3676–3680 (2015).
5. S. R. Koebley, F. Vollrath, H. C. Schniepp, Toughness-enhancing metastructure in the recluse spider's looped ribbon silk. *Mater. Horiz.* **4**, 377–382 (2017).
6. F. Zhu, L. Cheng, Z. J. Wang, W. Hong, Z. L. Wu, J. Yin, J. Qian, Q. Zheng, 3D-printed ultratough hydrogel structures with titin-like domains. *ACS Appl. Mater. Interfaces* **9**, 11363–11367 (2017).
7. T. T. T. Myllymäki, L. Lemetti, Nonappa, O. Ikkala, Hierarchical supramolecular cross-linking of polymers for biomimetic fracture energy dissipating sacrificial bonds and defect tolerance under mechanical loading. *ACS Macro Lett.* **6**, 210–214 (2017).
8. A. Rafsanjani, A. Akbarzadeh, D. Pasini, Snapping mechanical metamaterials under tension. *Adv. Mater.* **27**, 5931–5935 (2015).

9. B. Haghpanah, L. Salari-Sharif, P. Pourrajab, J. Hopkins, L. Valdevit, Multistable shape-reconfigurable architected materials. *Adv. Mater.* **28**, 7915–7920 (2016).
10. S. Shan, S. H. Kang, J. R. Raney, P. Wang, L. Fang, F. Candido, J. A. Lewis, K. Bertoldi, Multistable architected materials for trapping elastic strain energy. *Adv. Mater.* **27**, 4296–4301 (2015).
11. J. Wu, L.-H. Cai, D. A. Weitz, Tough self-healing elastomers by molecular enforced integration of covalent and reversible networks. *Adv. Mater.* **29**, 1702616 (2017).
12. E. Ducrot, Y. Chen, M. Bulters, R. P. Sijbesma, C. Creton, Toughening elastomers with sacrificial bonds and watching them break. *Science* **344**, 186–189 (2014).
13. S. C. Grindy, R. Learsch, D. Mozhdehi, J. Cheng, D. G. Barrett, Z. Guan, P. B. Messersmith, N. Holten-Andersen, Control of hierarchical polymer mechanics with bioinspired metal-coordination dynamics. *Nat. Mater.* **14**, 1210–1216 (2015).
14. E. Filippidi, T. R. Cristiani, C. D. Eisenbach, J. H. Waite, J. N. Israelachvili, B. K. Ahn, M. T. Valentine, Toughening elastomers using mussel-inspired iron-catechol complexes. *Science* **358**, 502–505 (2017).
15. R. Takahashi, T. L. Sun, Y. Saruwatari, T. Kurokawa, D. R. King, J. P. Gong, Creating stiff, tough, and functional hydrogel composites with low-melting-point alloys. *Adv. Mater.* **30**, 1706885 (2018).
16. X. Feng, Z. Ma, J. V. MacArthur, C. J. Giuffre, A. F. Bastawros, W. Hong, A highly stretchable double-network composite. *Soft Matter* **12**, 8999–9006 (2016).
17. X. Zheng, H. Lee, T. H. Weisgraber, M. Shusteff, J. DeOtte, E. B. Duoss, J. D. Kuntz, M. M. Biener, Q. Ge, J. A. Jackson, S. O. Kucheyev, N. X. Fang, C. M. Spadaccini, Ultralight, ultrastiff mechanical metamaterials. *Science* **344**, 1373–1377 (2014).
18. R. S. Lakes, T. Lee, A. Bersie, Y. C. Wang, Extreme damping in composite materials with negative-stiffness inclusions. *Nature* **410**, 565–567 (2001).
19. K. Bertoldi, P. M. Reis, S. Willshaw, T. Mullin, Negative Poisson's ratio behavior induced by an elastic instability. *Adv. Mater.* **22**, 361–366 (2010).
20. S. Babaee, J. Shim, J. C. Weaver, E. R. Chen, N. Patel, K. Bertoldi, 3D soft metamaterials with negative Poisson's ratio. *Adv. Mater.* **25**, 5044–5049 (2013).
21. B. Florijn, C. Coulais, M. van Hecke, Programmable mechanical metamaterials. *Phys. Rev. Lett.* **113**, 175503 (2014).
22. J.-H. Lee, L. Wang, M. C. Boyce, E. L. Thomas, Periodic bicontinuous composites for high specific energy absorption. *Nano Lett.* **12**, 4392–4396 (2012).
23. L. R. Meza, S. Das, J. R. Greer, Strong, lightweight, and recoverable three-dimensional ceramic nanolattices. *Science* **345**, 1322–1326 (2014).
24. G. X. Gu, M. Takaffoli, M. J. Buehler, Hierarchically enhanced impact resistance of bioinspired composites. *Adv. Mater.* **29**, 1700060 (2017).
25. Y. Ma, X. Feng, J. A. Rogers, Y. Huang, Y. Zhang, Design and application of 'J-shaped' stress–strain behavior in stretchable electronics: A review. *Lab Chip* **17**, 1689–1704 (2017).
26. T. Motokawa, Effects of ionic environment on viscosity of Triton-extracted catch connective tissue of a sea cucumber body wall. *Comp. Biochem. Physiol. B Comp. Biochem.* **109**, 613–622 (1994).
27. I. M. Van Meerbeek, B. C. Mac Murray, J. W. Kim, S. S. Robinson, P. X. Zou, M. N. Silberstein, R. F. Shepherd, Morphing metal and elastomer bicontinuous foams for reversible stiffness, shape memory, and self-healing soft machines. *Adv. Mater.* **28**, 2801–2806 (2016).
28. M. D. Dickey, Stretchable and soft electronics using liquid metals. *Adv. Mater.* **29**, 1606425 (2017).
29. S. Bauer, S. Bauer-Gogonea, I. Graz, M. Kaltenbrunner, C. Keplinger, R. Schwödiauer, 25th anniversary article: A soft future: From robots and sensor skin to energy harvesters. *Adv. Mater.* **26**, 149–162 (2014).
30. J. A. Rogers, T. Someya, Y. Huang, Materials and mechanics for stretchable electronics. *Science* **327**, 1603–1607 (2010).
31. Y. Lin, O. Gordon, M. R. Khan, N. Vasquez, J. Genzer, M. D. Dickey, Vacuum filling of complex microchannels with liquid metal. *Lab Chip* **17**, 3043–3050 (2017).
32. M. D. Dickey, R. C. Chiechi, R. J. Larsen, E. A. Weiss, D. A. Weitz, G. M. Whitesides, Eutectic gallium-indium (EGaIn): A liquid metal alloy for the formation of stable structures in microchannels at room temperature. *Adv. Funct. Mater.* **18**, 1097–1104 (2008).
33. V. Kochat, A. Samanta, Y. Zhang, S. Bhowmick, P. Manimunda, S. A. S. Asif, A. S. Stender, R. Vajtai, A. K. Singh, C. S. Tiwary, P. M. Ajayan, Atomically thin gallium layers from solid-melt exfoliation. *Sci. Adv.* **4**, e1701373 (2018).
34. S. Zhu, J.-H. So, R. Mays, S. Desai, W. R. Barnes, B. Pourdeyhimi, M. D. Dickey, Ultrastretchable fibers with metallic conductivity using a liquid metal alloy core. *Adv. Funct. Mater.* **23**, 2308–2314 (2013).
35. S. Shabahang, G. Tao, J. J. Kaufman, Y. Qiao, L. Wei, T. Bouchenot, A. P. Gordon, Y. Fink, Y. Bai, R. S. Hoy, A. F. Abouraddy, Controlled fragmentation of multimaterial fibres and films via polymer cold-drawing. *Nature* **534**, 529–533 (2016).
36. F. J. Spooner, C. G. Wilson, Slip and twinning in gallium. *J. Less Common Met.* **10**, 169–184 (1966).
37. K. R. Lyall, J. F. Cochran, Velocity of sound and acoustic attenuation in pure gallium single crystals. *Can. J. Phys.* **49**, 1075–1097 (1971).
38. S. Hashmi, *Comprehensive Materials Processing* (Elsevier, ed. 1, 2014).
39. C. G. Wilson, The plastic deformation of single crystals of gallium. *J. Less Common Met.* **5**, 245–257 (1963).
40. Z. Xue, J. W. Hutchinson, Neck retardation and enhanced energy absorption in metal–elastomer bilayers. *Mech. Mater.* **39**, 473–487 (2007).
41. Z. Ye, G. Z. Lum, S. Song, S. Rich, M. Sitti, Phase change of gallium enables highly reversible and switchable adhesion. *Adv. Mater.* **28**, 5088–5092 (2016).
42. F. Bachmann, R. Hielscher, H. Schaeben, Texture analysis with MTEX—Free and open source software toolbox. *Solid State Phenom.* **160**, 63–68 (2010).

Acknowledgments

Funding: We acknowledge support from the U.S. Army Natick Soldier Systems Center and the NSF (ERC EEC-1160483 and CMMI-1362284). **Author contributions:** M.D.D. conceived and designed the project. C.B.C., I.D.J., and D.P.P. carried out fabrication and characterization of the fibers. C.D.C. and R.M. modeled the fiber behavior. V.M.M. and J.N. completed the postmortem analysis of the fibers. C.B.C., M.D.D., and J.G. analyzed the results. C.B.C. and M.D.D. wrote the manuscript. All authors edited the manuscript. **Competing interests:** The authors declare that they have no competing interests. **Data and materials availability:** All data needed to evaluate the conclusions in the paper are present in the paper and/or the Supplementary Materials. Additional data related to this paper may be requested from the authors.

Submitted 4 March 2018
Accepted 11 January 2019
Published 22 February 2019
10.1126/sciadv.aat4600

Citation: C. B. Cooper, I. D. Joshipura, D. P. Parekh, J. Norkett, R. Mailen, V. M. Miller, J. Genzer, M. D. Dickey, Toughening stretchable fibers via serial fracturing of a metallic core. *Sci. Adv.* **5**, eaat4600 (2019).